IMPROVEMENT IN HARDNESS AND CORROSION RESISTANCE OF STEEL THROUGH RED MUD COATING

Bambang Sunendar Purwasasmita[1,2]*, Khalifa Aldila Putra[2], and Leanddas Nurdiwijayanto[2]

[1]Material Research Group, Material Engineering Study Program, Faculty of Mechanical and Aerospace, Institut Teknologi Bandung, Bandung, Indonesia

[2] Engineering Physics Research Group, Laboratory of Material Processing, Engineering Physics Study Program, Faculty of Industrial Technology, Institut Teknologi Bandung, Bandung, Indonesia,
Tel: +62-81-562-63888, *e-mail: purwa@tf.itb.ac.id

Received Date: November 11, 2010

Abstract

Red mud is a waste product produced during alumina extraction from bauxite by the Bayer's process and has become a major issue in connection with its disposal. As the aluminum demand in the world is increasing, the disposal of red mud waste into the environment also increases, bringing with its environmental issues coupled, however, a potential for the waste to generate a huge amount of unutilized resources still contained in the red mud, such as Fe_2O_3, Al_2O_3, SiO_2, and others. As a possible useful utilization of the disposable waste, red mud can be used as a fine ceramic coating material onto metal substrates. For a fine ceramic coating, fine red mud powder was mixed with other substances to form a non-aqueous coating slurry with toluene as the solvent, PEG 6000 as the binder and plasticizer, and sesame oil as the dispersant. The coating process was performed by a dip-coating method onto ST-37 steel with a withdrawal speed of 0.23 mm/sec. The densification of coating material took place after calcinations at 900 °C, 1100 °C, and 1300 °C for 2 hours in nitrogen atmosphere. This treatment evinced an improvement of the surface hardness from 146.2 HV to 1738.8 HV for the sample calcined at 1100°C and the corrosion resistance by 4.14 times, for the sample calcined at 1300°C.

Keywords: Ceramic coating, Corrosion resistance, Hardness, Non-aqueous coating slurry, Red mud

Introduction

The production of aluminum metal from bauxite commercially comprises of two processing steps, namely the extraction of alumina from bauxite by the Bayer's process [1] and the electrolyzation of alumina in a Hall-Heroult cell [2]. The waste by-product of the alumina extraction from bauxite is known as red mud. Through the Bayer's process, approximate 35-40% of the processed bauxite goes into red mud waste and becomes the biggest problem in alumina production because it generally exits the process stream as a highly alkaline slurry (pH 10-12.5) containing about 15-30% solids [3,4,5]. About 90 million metric tons of red mud are produced each year [6]. This huge amount of waste makes serious problems to the waste storage due to the need of large waste reservoirs and it will also impose an environmental impact. The red mud still contains important materials for industrial processes, such as Fe_2O_3 (30-60 wt%), Al_2O_3 (10-20 wt%), SiO_2 (3-50 wt%), Na_2O (2-10 wt%), CaO (2-8 wt%), and TiO_2 (0-25 wt%). Therefore, many researches had been conducted to utilize red mud for various applications, such as wastewater treatment for removing toxic metals [3,7,8], building materials [4,9], adsorbents, and catalysts [5].

Although many researches and developments have been conducted on the utilization of red mud, there were almost no attempts on the utilization of red mud waste for surface modification. The utilization of red mud for surface modification onto metal substrates had been reported by Satapathy et. al. through plasma spray coating onto various metal

substrates [10]. They used sieved red mud waste to obtain particle size of about 60-100 microns. The coating was performed by plasma spraying over aluminum, copper, mild steel, and stainless steel substrates with various applied torch input powers. By this method, the maximum hardness achieved was 560 HV.

Since there were almost no attempts on the utilization of red mud waste for surface modification, this research was aimed at utilizing red mud for surface modification. The coating was expected to improve the surface hardness and corrosion resistance of steel. In industrial processes, the hardness of steel is usually improved by alloying with increasing amount of noble metals, such as chromium, nickel, titanium, vanadium, etc. Alloying with such noble metals will indeed increase its price. Meanwhile, the corrosion protection in industrial processes was usually achieved by cathodic protection. However, this method is quite expensive although it offers good corrosion resistance. The coating by red mud through a chemical solution process, as is reported in this paper, can probably give an alternative for industrial scale applications by a relatively inexpensive and simple method. However, this method still needs further research and development to ascertain all the properties and behaviors of red mud-coated steel. In this research, the coating method was different from that in the work of Satapathy et. al. The coating of red mud was performed onto ST-37 steel through a dip-coating method. The coated steel was characterized using x-ray diffraction (XRD), scanning electron microscopy (SEM), energy dispersive spectroscopy (EDS), Vickers microhardness, and corrosion test by a weight loss method in 10% H_2SO_4 solution. The results showed improvements of corrosion protection and surface hardness of the coated steel. The maximum surface hardness of 1738.8 HV obtained was higher than that reported by Satapathy et. al. [10] although the method used was simpler.

Experiment

The red mud used in this research was obtained from the extraction of alumina from bauxite ore in West Kalimantan, Indonesia. Table 1 below shows the elements contained in the red mud are predominantly 32.77% Al_2O_3 and 37.58% Fe_2O_3 in mass percentage. A non-aqueous coating precursor was produced from a mixture of red mud powder, toluene as solvent, and polyethylene glycol 6000 (PEG 6000) as binder and plasticizer. Sesame oil was used as dispersant to prevent the agglomeration of red mud powder. The ratio of toluene and sesame oil as the liquid phase of the non-aqueous coating precursor was set at 59.1:40.9 %v/v, and the ratio of red mud powder and binder & plasticizer as solid phase was set at 99.97:0.03 at %wt/wt. Both phases, namely the liquid phase and the solid phase, were mixed with composition of 7 ml of liquid and 3 g of solid. Mixing was carried out by means of an ultra-turrax homogenizer at 20000 rpm for 10 minutes for each mixing step.

Table 1. Elemental Composition of Red Mud by X-ray Fluorescence

No.	Elements	Content (%wt/wt)	No.	Elements	Content (%wt/wt)
1	Al_2O_3	32.77	6	Na_2O	3.03
2	Fe_2O_3	37.58	7	MnO	0.16
3	H_2O	19.33	8	MgO	0.14
4	TiO_2	3.43	9	P_2O_5	0.09
5	SiO_2	3.40	10	CaO	0.06

ST-37 steel was used as the substrate and it was polished using a 2000 grit sandpaper, cleaned ultrasonically with detergent, acetone, and methanol, each for 5 minutes and then dried at ambient temperature to remove fat from the substrate. For complete cleaning of the metal substrate, the substrate was immersed in 1M NaOH for 10 minutes and rinsed with distilled water. The substrate was then immersed in 1M HCl for 10 minutes to improve its surface roughness and further rinsed with distilled water before being dried at ambient temperature. The coating process was carried out by a dip-coating method with a withdrawal speed of 0.23 mm/sec. The coating process was performed only once. The calcination process at 900, 1100, and 1300ºC for 2 hours was carried out in nitrogen atmosphere to improve the morphology, crystallinity and chemical properties of the coating layer. Characterization was done using XRD (Philips Analitical X-Ray, Cu Kα, λ=1.54060 Å) to examine the phases in the coating, SEM (JEOL JSM 6360LA Analytical SEM) to examine morphology of the layer, and EDS (JEOL JSM 6360LA) to examine elemental percentage of the probed area. The surface hardness of the prepared sample was examined by means of a micro Vickers hardness tester (Shimadzu Corporate M-85055) with 0.5 kg_f load for 15 seconds. The corrosion test was carried out by a weight loss method using 10% H_2SO_4 as the corrosion medium for 1, 3, 5, and 7 days. The samples were then cleaned from the corrosion products using continuous flowing water, immersed in acetone, and then dried in ambient condition. The corrosion rate (*CR*) can be calculated using the following formula [11],

$$CR = \frac{K.W}{A.T.D} \tag{1}$$

where K is a constant (8.76×10^4 mm/year), W is the weight loss (g), T is the immersion time (hours), A is the area of the sample (cm^2), and D is the density of the sample (g/cm^3).

Result and Discussion

Figure 1 shows the XRD pattern of untreated red mud. From this XRD result, it can be seen that the red mud has gibbsite (α-$Al(OH)_3$) and goethite (α-FeOOH) crystalline phases. The gibbsite shows the highest intensity that indicates the gibbsite has the highest content in this mixture phases. The other compounds composed by elements other than Al and Fe in Table 1 such as TiO_2 and SiO_2 are not detected. It was probably caused by the amorphous phase or the small amount of those compounds. The crystalline phases of Al_2O_3 and Fe_2O_3 are also not detected. The XRD result of this red mud is different than that has been reported by Yalçin et. al. [12] and Castaldi et. al. [13]. The red mud used in this experiment was composed by crystalline phases of two hydroxide-based compounds. On the contrary, the red mud used by Yalçin et. al. and Castaldi et. al. had crystalline phases of oxide-based compounds, namely hematite (α-Fe_2O_3), iron titanium oxide (Fe_2TiO_5), sodalite ($Na_8(Cl,OH)_2Al_6Si_6O_{24}$) and cancrinite ($Na_6Ca_{1.5}Al_6Si_6O_{24}(CO_3)_{1.6}$). The crystalline phase compounds contained in the red mud depend on its mineral resources, mineral resource's geography and their environmental condition. That is why the red mud has different crystalline phase compounds and compositions depending on their origin location.

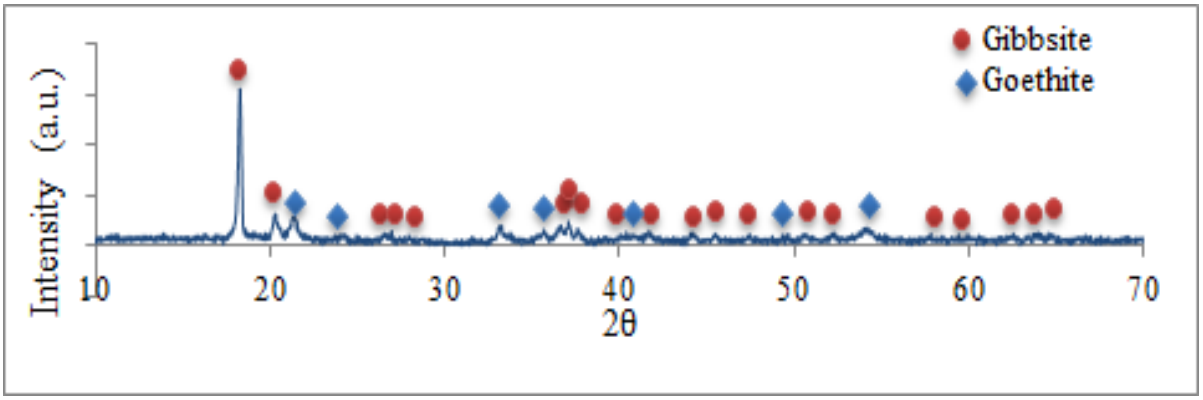

Figure 1. XRD pattern of untreated red mud

Figure 2 shows the XRD pattern of coated samples with different calcination temperatures. It can be seen that each temperature shows different phase formation. Single-phase formation is detected for the sample calcined at 900 °C showing the formation of wustite (FeO). On the contrary, samples calcined at 1100 °C and 1300 °C show multiphase formation, where the sample calcined at 1100 °C shows the formation of wustite (FeO), magnetite (Fe_3O_4), maghemite (γ-Fe_2O_3) and c orundum (α-Al_2O_3). Meanwhile, the sample calcined at 1300 °C shows the formation of magnetite (Fe_3O_4), corundum (Al_2O_3), ulvospinel ($TiFe_2O_4$) and ilmenite ($FeTiO_3$).

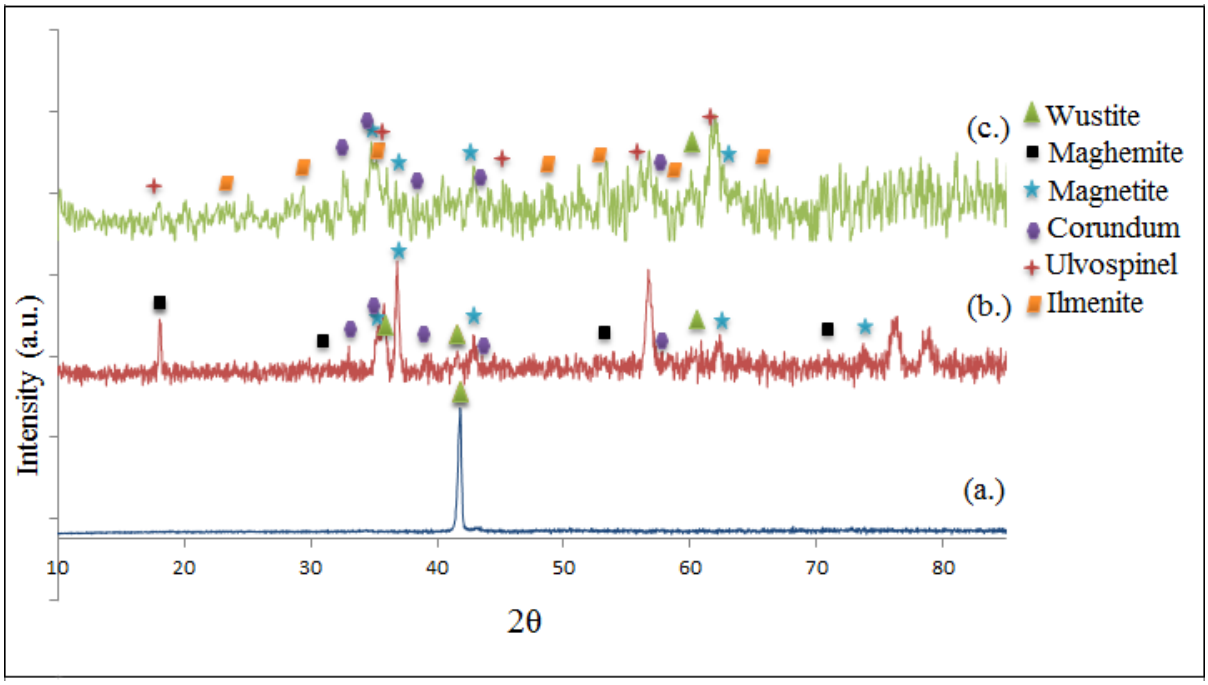

Figure 2. XRD patterns of prepared samples with different calcination temperatures: (a.) 900 °C, (b.) 1100 °C and (c.) 1300 °C

Red mud consists of several elements and complex compounds, therefore after the calcination process, formation of several phases may appear. Fe2O3 is one of main elements of red mud discharged by the Bayer's process (see Table 1), which appear in the form of goethite that give sorrel color to the red mud. After the calcination process, the sorrel color of red mud transformed to a metallic color, which indicated the occurrence of a reduction mechanism of Fe3+ to Fe2+ [14]. In this case, Fe2O3 transformed to FeO. When the heat treatment was performed to the red mud, the goethite transformed to hematite (α-Fe2O3) when the temperature reached 300 °C [15]. Along with the increase of the temperature, Fe2O3 was easily reduced to FeO when the calcination was carried out at least at 900 °C together with the organic compound that have functional groups of carbon and sulfur according to the reaction mechanism as follows:

$$Fe_2O_{3(s)} + CO_{(g)} \rightarrow 2FeO_{(s)} + CO_{2(g)} \quad (2)$$

FeO is an iron oxide and easily transforms to Fe_3O_4 at higher heat treatment temperatures above 900 °C. At the calcination temperature over 1000 °C, FeO has the tendency to bring about the formation of titanium-ferrite oxide compounds if the composition contains TiO_2 [14,16]. Since red mud contains 3.77% of TiO_2, therefore the sample calcined at 1300°C shows the appearance of titanium-ferrite oxide compounds, namely ulvospinel and ilmenite.

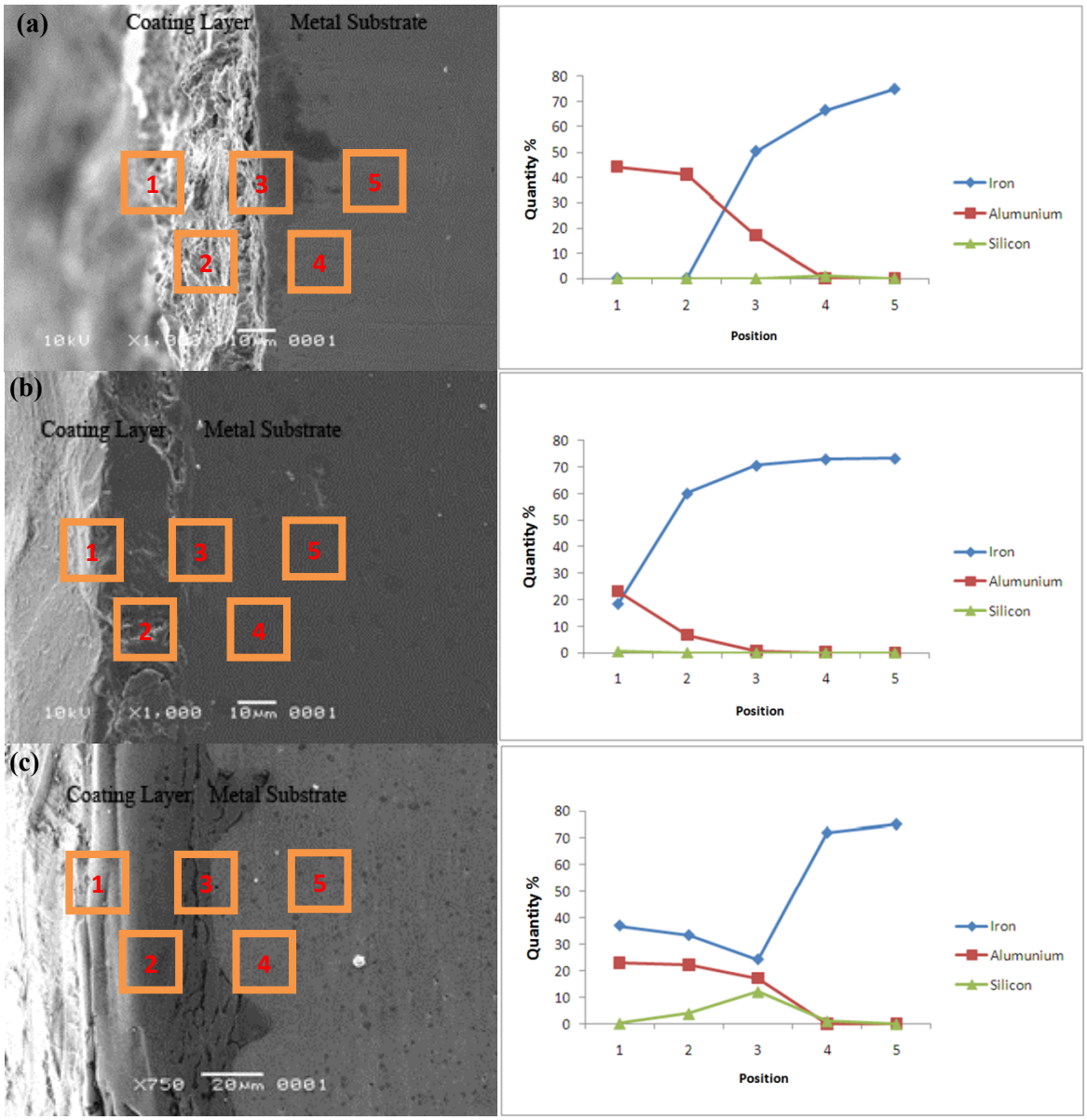

Figure 3. Cross-section SEM of calcined samples and EDS result of spotted area, (a) 900° C, (b) 1100°C, and (c) 1300°C

The cross-section SEM micrographs and the curves of EDS results of three elements, namely iron, aluminum and silicon at the probed areas marked by number 1 to 5 are shown in Figure 3. Area 1 is the area of the surface layer of the red mud coating, area 2 is the coating layer of the red mud coating, area 3 is the interface layer between the coating layer and the substrate, area 4 and area 5 are the ST-37 steel substrate. The area 4 is much closer to the interface layer than that of area 5. From the EDS results, a trend can be seen where there is an increase of iron content from area 1 to 5 and a decrease of aluminum content from area 1 to 5. These results show a proof on diffusion mechanism of iron from surface layer to interface layer and the diffusion mechanism of aluminum from interface layer to surface layer. As the increase of calcination temperature takes place, the movement of atoms becomes free, and thus they more easily diffuse. As a result, the low-density elements will diffuse to the surface layer and the high-density elements will diffuse as if sinking forward to the substrate. The content of silicon is very small for all calcined

samples, approximately below 1%. However, for the sample calcined at 1300°C, the quantity of silicon is near 12% at area 3. The relatively high amount of silicon at area 3 was caused by the melting of amorphous silica that diffused forward to the substrate. The melting of amorphous silica also led to the displacement of other compounds such as corundum and magnetite into the substrate. It is proven from EDS that there is an increase of Al amount at areas 2 and 3 when the calcination temperature increases from 1100°C to 1300°C (Figure 3(b) and 3(c)), and there is a decrease of Fe amount at areas 2 to 3 for sample calcined at 1300°C (Figure 3(c)). The diffusion of melted amorphous silica to the substrate has also been reported by Purwasasmita et. al. [17,18]. They reported that the amorphous silica melted at relatively low temperature, i.e. 850°C, and further diffused forward to the substrate that comprise of $Pb(Zr_{0.53}Ti_{0.47})O_3$ and $BaTiO_3$ ceramics.

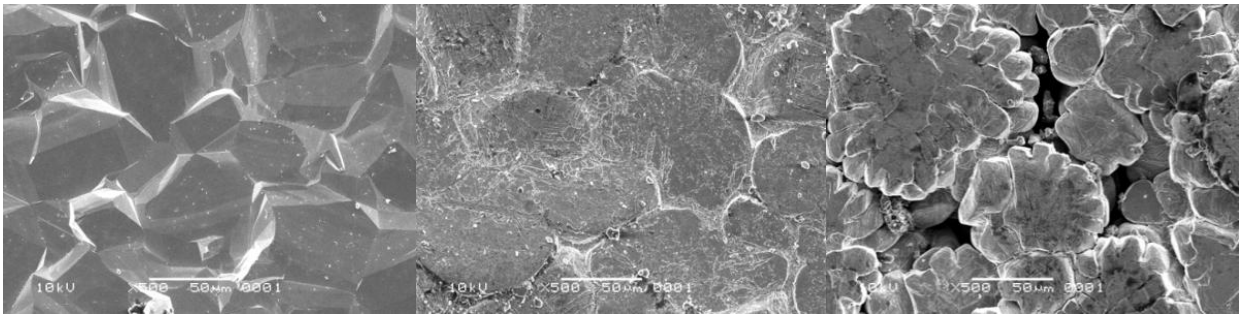

(a) **(b)** **(c)**

Figure 4. SEM micrograph of prepared samples calcined at: (a.) 900°C, (b.) 1100°C, (c.) 1300°C

The surface morphologies corresponding to various calcination temperatures are shown in Figure 4. From the SEM micrographs, it can be seen that as the temperature increases, the grain boundary in the coating surface is more visible. The element diffusion forward to substrate as the temperature increased was the main factor causing the visibility of grain boundary. The diffusion of elements forward to the substrate results in vacancies on surface layer due to the melting of amorphous silica that diffuses forward to the substrate and creates the interface layer between coating layer and substrate. At the calcination temperature of 900°C, amorphous silica did not melt well, but as the temperature increased, silica played an important role in binding the other compounds. However, when the temperature caused the amorphous silica to be completely molten, it would sink forward to substrate and made the binding among other compounds on the surface layer descend. It was shown by the more compact and denser of surface morphology of the sample calcined at 900°C and 1100°C than that of sample calcined at 1300°C. In sample calcined at 1300°C, amorphous silica melted, diffused forward to substrate, and settled in interface layer, and thus results in vacancies on surface layer. The settled of silica ininterface layer can be detected by EDS of sample calcined at 1300°C, in which it shows high content of Si at area 3 (Figure 3(c)).

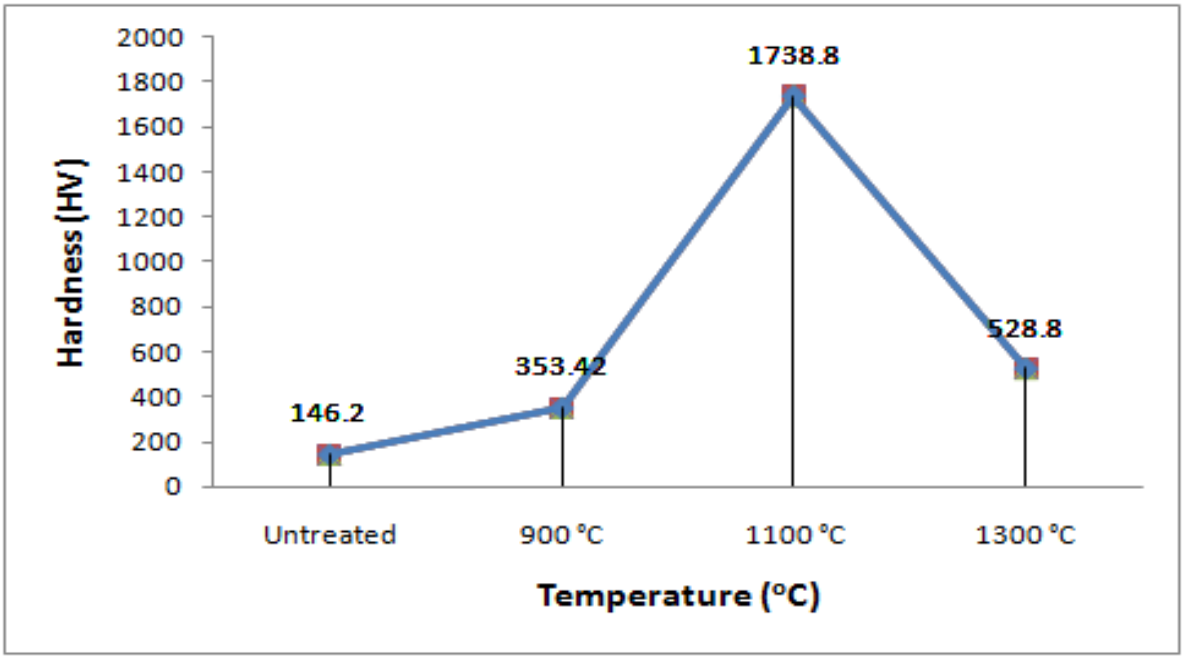

Figure 5. The Vickers hardness of prepared samples at various calcined temperatures

Figure 5 shows a curve of Vickers hardness of samples calcined at various temperatures. This result shows a trend of increasing the surface hardness as the temperature increases. The maximum surface hardness is 1738.8 HV for sample calcined at 1100°C. The increase of surface hardness as the temperature increases is mainly attributed to both the phase formation and the diffusion of each compound particles that leads to the formation of better crystallinity of the phase formed on coating layer. When the heat treatment is carried out, the diffusion mechanism occurs between red mud particles and substrate, and the diffusion among red mud particles itself. The heat treatment process also influences the phase formation of coating layer. Every phase has its hardness characteristic, such as FeO has a hardness range of about 250-350 HV, Fe_3O_4 has 450-550 HV, Fe_2O_3 has a hardness value of more than 1000 HV [19], Al_2O_3 has 1800 HV, $TiFe_2O_4$ has 650 HV, and $FeTiO_3$ has 566-698 HV. The hardness characteristic of every phase will contribute to the increase of surface hardness depending on the dominant phase formed, where the high crystallinity of the dominant phase formed on the coating layer diffuse with each other and substrate to form a dense coating layer. As shown by the XRD result, the sample calcined at 1100°C had the best crystallinity as shown by the sharp peaks dominated by magnetite, maghemite and corundum. Since at the calcination temperature of 1100°C the amorphous silica contained in the red mud did not melt well, the phase of magnetite, maghemite and corundum will be bound with silica by creating necking mechanism between silica and those of other compounds. The role of silica here is to create a binding among those compounds to form a dense surface layer. Therefore, the hardness of sample calcined at 1100°C shows the highest value. When the calcination temperature increases to 1300°C, silica contained in the red mud melts as glass liquid, diffused forward to the substrate, and settled in interface layer. Therefore, the bond among those compounds in the surface layer decreases, and thus, the surface hardness decreased although the intensity of the corundum phase increases.

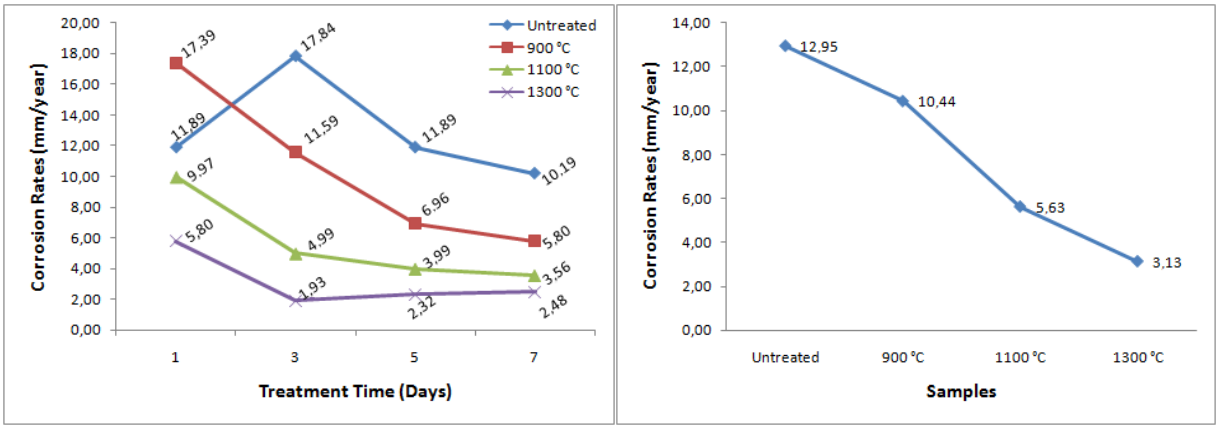

(a) **(b)**

Figure 6. (a) Corrosion rate treated by a weight loss method for several days, (b) Average corrosion rate of calcined samples for 7 days

Figure 6 shows the corrosion rate of untreated and red mud coating treated samples for several days and the average of corrosion rate for 7 days by a weight loss method in 10% H_2SO_4 solution. From Figure 6(a), it can be seen that the corrosion rate has a tendency to decrease over time. It happens because at the beginning when soaked into acid solution, steel originally looks for its stable form. The stable form occurs when the corrosion product is formed over the entire surface. When the entire surface is already coated by corrosion products, the steel becomes more stable and the corrosion rate will decrease. The corrosion rate of untreated sample showed an increase profile on the first day to the third day. The increase of corrosion rate was caused by the formation of more stable passive layer of corrosion product on the first day but the passive layer fell on the next day. Thus, the corrosion layer would be formed again after the passive layer had fallen until the third day. From Figure 6(b), it can be seen that, the average corrosion rate decreases as the calcination temperature increases. The best corrosion rate is shown by the sample calcined at 1300°C with an average value of 3.13 mm/year. This value is 4.14 times better than that for the untreated sample, 12.95 mm/year. The decrease of the average corrosion rate as the temperature increases is caused by both the formation of corrosion resistant phases and better densification of the interface layer when calcined at higher temperatures. The formation of more stable phases such as Fe_2O_3, Fe_3O_4 and $TiFe_2O_4$ will lead to the better corrosion resistance. In addition, the melting of one compound at relatively high calcination temperature also contributes to the decrease of the average corrosion rate. At high temperatures, the amorphous silica contained in the red mud melts and diffuses forward into the substrate and creates an interface between the substrate and the coating layer. As a result, the melted silica filled the vacancies in the interface layer between the coating layer and the substrate.

Conclusions

The surface modification on ST-37 steel has been successfully carried out by coating with red mud. The coating was aimed to improve the surface hardness and corrosion resistance of steel. By this treatment, the best surface hardness was achieved for red mud-coated steel calcined at 1100°C with a Vickers hardness of 1738.8 HV, 11.9 times better than that of untreated steel. The increase of surface hardness as the temperature increases is attributed to the formation of corrosion resistant oxide phases and the diffusion of each compound leading to an increase in crystallinity of the phases formed in the coating layer. The

diffusion between atoms in the red mud and the substrate induced by heat treatment at appropriate temperatures will also lead to the increase in surface hardness due to the formation of a denser coating layer. Generally, corrosion test results by a weight loss method for all samples show a tendency to decrease over time. The optimum average corrosion rate was 3.13 mm/year for sample calcined at 1300°C, 4.14 times lower than that of untreated sample. The decrease of average corrosion rate as the temperature increases is caused by a better densification in the interface layer between the coating layer and the substrate, because at higher temperatures, the amorphous silica melts and fills the vacancies in the interface layer, and thus will make better cover over steel surface.

References

[1] A.R. Hind, S.K. Bhargava, and S.C. Grocott, "The surface chemistry of buyer process solid: A review," *Colloids and Surfaces Aspect*, Vol. 146, pp. 359-374, 1999.

[2] C.M. Hall, "Process of reducing aluminium by electrolysis ," US Patent 400766, 1889.

[3] A.I. Zouboulis, and K.A. Kydros, "Use of red mud for toxic metal removal: The case of nickel," *Journal of Chemical Technology and Biotechnology*, Vol. 53, pp. 95-101, 1993.

[4] P.E. Tsakiridis, S. Agatzini-Leonardou, and P. Oustakadis, "Red mud addition in the raw meal for the production of Portland cement clinker," *Journal of Hazardous Materials B*, Vol. 116, pp. 103-110, 2004.

[5] S. Wang, H.M. Ang, and M.O. Tadé, "Novel application of red mud as coagulant, adsorbent and catalyst for environmentally benign processes," *Chemospher*, Vol. 72, pp. 1621-1635, 2008.

[6] S. Kumar, R. Kumar, and A. Bandopadhyay, "Innovative methodologies for the utilization of wastes from metallurgical and allied industries," *Resources, Conservation and Recycling*, Vol. 48, pp. 301-314, 2006.

[7] H. Genç-Furman, J.C. Tjell, and D. McConchie, "Adsorption of arsenic from water using activated neutralized red mud," *Journal of Environmental, Science and Technology*, Vol. 38, pp. 2428-2434, 2004.

[8] V.K. Gupta, and S. Sharma, "Removal of cadmium and zinc from aqueous solution using red mud," *Journal of Environmental, Science and Technology*, Vol. 36, pp. 3612-3617, 2002.

[9] M. Singh, S.N. Upadhayay, and P.M. Prasad, "Preparation of special cement from red mud," *Journal of Waste Management*, Vol. 16, No. 8, pp. 665-670, 1996.

[10] A. Satapathy, S.C. Mishra, P.V. Ananthapadmanabhan, and K.P. Sreekumar, "Development of ceramic coatings using red mud – A solid waste of alumina plants," *Journal of Solid Waste Technology and Management*, Vol. 33, No. 2, pp. 48-53, 2007.

[11] American Society for Testing and Materials (ASTM), *Standard Practice for Preparing, Cleaning and Evaluating Corrosion Test Specimens (ASTM G1 90(1999)e1)*, West Conshohocken, Pennsylvania, United States, 1999.

[12] N. Yalçin and V. Sevinç, "Utilization of bauxite waste in ceramic glazes," *Ceramics International*, Vol. 26, pp. 485-493, 2000.

[13] P. Castaldy, M. Silvetti, L. Santona, S. Enzo, and P. Melis, "XRD, FTIR and thermal analysis of bauxite ore-processing waste (red mud) exchanged with heavy metals," *Clays and Clay Minerals*, Vol. 56, No. 4, pp. 461-469, 2008.

[14] D.C. Presnall, "Phases Diagrams of Earth-Forming Minerals," In *Mineral Physics & Crystallography: A Handbook of Physics Constant*, T.J. Ahrens, ed.: American Geophysical Union, Washington D.C., United States, pp. 248-268, 1995.

[15] S. Gialanella, F. Girardi, G. Ischia, I. Lonardelli, M. Mattarelli, and M. Montagna, "On the goethite to hematite phase transformation," *Journal of Thermal Analysis and Calorimetry*, Vol. 102, No. 3, pp. 867-873, 2010.
[16] L.A. Tailor, R.J. Williams, and R.H. McCallister, "Stability relations of ilmenite and ulvospinel in the Fe-Ti-O system and application of these data to lunar mineral assemblages," *Journal of Earth and Planetary Science Letters*, Vol. 16, No. 2, pp. 282-288, 1972.
[17] B.S. Purwasasmita, and T. Kimura, "Effect of glass composition on chemical reaction between Lead Zirconate Titanate and glasses. (Part 1). Lead-Borate glasses," *Journal of the Ceramic Society of Japan*, Vol. 108, No. 1263, pp. 966-972, 2000.
[18] B.S. Purwasasmita, and T. Kimura, "Effect of glass composition on chemical reaction between Lead Zirconate Titanate and glasses. (Part 2). Lead-silicate and Lead-borosilicate glasses," *Journal of the Ceramic Society of Japan*, Vol. 109, No. 1265, pp. 4-8, 2001.
[19] L.E. Samuels, *Light Microscopy of Carbon Steel*, American Society for Metals (ASM) International, United States, 1999.